Progressive Recruitment of the Frontoparietal Multiple-demand System with Increased Task Complexity, Time Pressure, and Reward

Sneha Shashidhara[1], Daniel J. Mitchell[1], Yaara Erez[1], and John Duncan[1,2]

Abstract

■ A distributed, frontoparietal "multiple-demand" (MD) network is involved in tasks of many different kinds. Integrated activity across this network may be needed to bind together the multiple features of a mental control program (Duncan, 2013). Previous data suggest that, especially with low cognitive load, there may be some differentiation between MD regions (e.g., anterior vs. posterior regions of lateral frontal cortex), but with increasing load, there is progressive recruitment of the entire network. Differentiation may reflect preferential access to different task features, whereas co-recruitment may reflect information exchange and integration. To examine these patterns, we used manipulations of complexity, time pressure, and reward while participants solved a spatial maze. Complexity was manipulated by combining two simple tasks. Time pressure was added by fading away the maze during route planning, and on some of these trials, there was the further possibility of a substantial reward. Simple tasks evoked activity only in posterior MD regions, including posterior lateral frontal cortex, pre-supplementary motor area/anterior cingulate, and intraparietal sulcus. With increasing complexity, time pressure, and reward, increases in activity were broadly distributed across the MD network, though with quantitative variations. Across the MD network, the results show a degree of functional differentiation, especially at low load, but strong co-recruitment with increased challenge or incentive. ■

INTRODUCTION

A set of frontal and parietal brain regions, collectively termed the multiple-demand (MD) network, is recruited during performance of a wide range of cognitive activities (Duncan & Owen, 2000). Included in this network are several distinct regions of the lateral frontal cortex (LFC), the anterior insula and the adjacent frontal operculum (AI/FO), the pre-supplementary motor area and the adjacent dorsal anterior cingulate cortex (preSMA/ACC), and the intraparietal sulcus (IPS; Duncan, 2010). To explain involvement in tasks of many different kinds, we have proposed a role in constructing mental control programs (Duncan, 2010, 2013). In general, each step of a complex task requires assembly of multiple cognitive fragments, appropriately related and bound to their roles. Through widespread connections throughout the brain, MD regions may play a central role in constructing such "attentional episodes" (Duncan, 2013).

Though MD activity increases with many kinds of task difficulty (Camilleri et al., 2018; Fedorenko, Duncan, & Kanwisher, 2013; Duncan, 2006; Nyberg et al., 2003), it is unclear how its component regions function individually and together to address cognitive challenges. Some prior data suggest a pattern of partial differentiation between MD regions at low cognitive load, which progressively disappears as load increases (Duncan, 2001). In verbal tasks, for example, MD activity may be stronger in the left hemisphere at low load, but increasingly bilateral as load increases (Rottschy et al., 2012; Wager & Smith, 2003). On the lateral frontal surface, various findings suggest progressive anterior spread of activity as task rules become more hierarchical or complex (Badre & Nee, 2018; Crittenden & Duncan, 2014; Badre & D'Esposito, 2007, 2009; Badre, 2008). More broadly, there have been many suggestions of relative functional specializations for different MD regions, though with little consensus emerging across studies (Yeo et al., 2015; Hampshire, Thompson, Duncan, & Owen, 2011; Nomura et al., 2010; Dosenbach et al., 2007). A combination of relative specialization but also substantial co-recruitment is expected if MD regions link together multiple cognitive contents into attentional episodes. An attentional episode will be a rich cognitive structure, combining linked stimulus inputs, goals, information from semantic memory, potential actions and rewards, and so forth. Given their different connectivity, MD regions will differ in their immediate access to these different domains of information, opening the door to relative specialization in tasks

[1]MRC Cognition and Brain Sciences Unit, Cambridge, UK, [2]University of Oxford

Journal of Cognitive Neuroscience 31:11, pp. 1617–1630
https://doi.org/10.1162/jocn_a_01440

with different content (Duncan, 2001). Such relative specialization may be especially visible at low load. Linking information into the correct structures, however, will require substantial information exchange and integration, suggesting widespread co-recruitment. Co-recruitment of the entire network may become most visible as load and overall activity increase. Relative specialization accompanied by substantial information exchange is also suggested by studies using multivoxel pattern analysis, with relevant task features widely decodable across MD regions, but with some quantitative differentiations (Cole, Ito, & Braver, 2016; Crittenden, Mitchell, & Duncan, 2016; Woolgar, Jackson, & Duncan, 2016).

In this study, we used a maze task to study patterns of specialization and spread across a set of a priori MD regions defined by common response to diverse task demands (Fedorenko et al., 2013). In the simplest task versions, participants either planned a four-move route in a spatial maze or responded to two arrows that accompanied the maze. In these simple conditions, we expected the strongest evidence for differentiation between MD regions. Two MD regions, in particular, the posterior-dorsal LFC (pdLFC) and the IPS, have especially strong links to spatial processing, including eye movements, with the MD region in pdLFC lying close to the location of the human FEF (Corbetta et al., 1998; Pierrot-Deseilligny, Rivaud, Gaymard, & Agid, 1991). Thus, we expected strong activity in IPS and pdLFC even for the simple tasks and recorded saccades to assess their potential contribution to such activity.

Next, we wished to examine the effects of increased task complexity. Though complexity is a broad term, here we considered simply the number of items or cognitive operations involved in the task. On this definition, there is much evidence that increased task complexity drives increased activity across the entire MD network, for example, with increasing n in *n*-back working memory tasks (Hampshire, Highfield, Parkin, & Owen, 2012; Hampshire et al., 2011; Postle, Berger, & D'Esposito, 1999; Owen, 1997). To increase complexity, we required maze and arrow tasks to be solved simultaneously. Within the MD network, we expected activity to strengthen and extend with increasing complexity. In particular, following prior results related to rule complexity (Crittenden & Duncan, 2014; Badre & D'Esposito, 2007, 2009), we expected increasing anterior spread along LFC.

To compare with complexity, we used two further manipulations. The first was time pressure, chosen as a candidate for enhancing the sense of challenge and accompanying autonomic arousal. Activity in several MD regions, for example, insula and ACC, has been shown to correlate with increasing blood pressure, during both *n*-back working memory tasks and tasks where participants were told to apply physical pressure (Critchley et al., 2003). Such results have been used to link activity to cognitive effort and autonomic arousal. Supporting a link to autonomic function, activity in similar MD regions is correlated with accuracy in a heartbeat detection task (Critchley, Wiens, Rotshtein, Öhman, & Dolan, 2004). Subjective reports during electrical stimulation of ACC can include a sense of impending challenge and the need to overcome it (Parvizi, Rangarajan, Shirer, Desai, & Greicius, 2013). Here, we manipulated time pressure by comparing self-paced problem solving with problems visible only for a restricted time.

Our final manipulation was reward. ACC has been studied extensively in the context of reward processing (Shenhav, Botvinick, & Cohen, 2013; Rushworth, Walton, Kennerley, & Bannerman, 2004). In the behaving monkey, ACC neurons code multiple aspects of reward prediction and receipt (Matsumoto, Suzuki, & Tanaka, 2015; Kennerley & Wallis, 2009; Hadland, Rushworth, Gaffan, & Passingham, 2003; Procyk, Ford Dominey, Amiez, & Joseph, 2000). In human fMRI, ACC activity increases with reward magnitude (Knutson, Taylor, Kaufman, Peterson, & Glover, 2005), though strong effects of reward can also be seen in many other MD regions (Botvinick & Braver, 2015; Dixon & Christoff, 2012; Padmala & Pessoa, 2011). To compare reward effects across MD regions, on some trials we added the possibility of a substantial monetary reward.

In line with a link to autonomic function, pupil size has been correlated with activity in insula and other MD regions (Paulus et al., 2015). In general, pupil size increases with cognitive load (Alnaes et al., 2014; Zekveld, Rudner, Kramer, Lyzenga, & Rönnberg, 2014) and has also been correlated with speed pressure (Murphy, Boonstra, & Nieuwenhuis, 2016) and reward magnitude (Muhammed et al., 2016; Gergelyfi, Jacob, Olivier, & Zénon, 2015; Chiew & Braver, 2014). Here, we measured changes in pupil size for each of our task manipulations and compared profiles of MD activity with profiles of pupil dilation.

In summary, in the context of planning solutions to a spatial maze, we examined manipulations of complexity, time pressure, and reward. Across these three manipulations, our aim was to examine similarities and differences in the pattern of strengthening and extension of activity across the MD network.

METHODS

Participants

Twenty-five participants (13 women) between the ages of 18 and 40 years (M = 27 years) took part in the study. One was excluded, owing to his falling asleep in the scanner. A sample size of 24 was determined before data collection, as typical for functional imaging studies. All participants were right-handed with normal or corrected-to-normal vision and had no history of neurological or psychiatric illness. To avoid interference with pupil measurement, participants with glasses were avoided, but participants with contact lenses were allowed. The study was conducted with approval by the Cambridge Psychology

Research Ethics Committee. All participants gave written informed consent and were reimbursed for their time.

Task Details

Participants had to solve a simple maze task and variations of it in the scanner (Figure 1A). They had to plan a route from a start location (marked by a green dot) to a goal location (marked by a magenta dot), avoiding blocked paths. The goal location was always at one of the four corners of the 4×4 maze; the start location was either in one of the central four positions (Figure 1B, left) or in an edge position (Figure 1B, right), such that the correct route always required four steps, including one, two, or three turns. In trials with a central start, there were five path blocks: three around the start dot, one around the goal, and one in between. In the case of an edge start, there were four path blocks: two around the start, one around the goal, and one in between. The maze spanned 15.2° visual angle horizontally and 10° vertically. Start and goal dots were 0.5° visual angle in diameter. Each trial was split into planning and execution phases (Figure 1A). In the planning phase, the maze was presented, and participants generated their route and then pressed a button to indicate that the plan was complete. There followed a fixed delay of 2 sec and then, on 25% of trials only, an execution phase. On these trials, the maze reappeared, but without the blocked paths. Participants used their previously planned route to move the green dot from the start position to the goal. Omission of blocked paths ensured that the previously planned route had to be remembered and used. Participants moved the green dot in the maze in any of the four directions using a custom-made button box with four buttons arranged like the arrow keys on a keyboard. Note that, for fMRI analysis, we focused just on planning phase data; execution was required on a subset of trials simply to ensure that participants did plan as instructed. As the occurrence of the execution phase was unpredictable, our design ensured that routes were planned on all trials, confirmed by high accuracy when execution was required (see Results).

There were six different conditions, each indicated by a 1-sec written cue at trial onset, followed by a 1-sec interval and then the maze for the planning phase. In the baseline condition (cue "none"), the planning phase was a maze without start and goal dots or blocked paths, which appeared for 1 sec and then disappeared. Participants had to press a button after the maze disappeared. They were instructed to do this as soon as possible. There were no baseline trials with execution, as there was no problem to be solved in this condition. In the simple maze condition (cue "maze"), participants carried out the maze task as described above. In the simple arrow condition (cue "arrow"), the baseline maze appeared with two arrows (0.27° visual angle) on either side of the maze. Each arrow pointed in one of four directions—up, down, left, or right. Participants pressed a button once they had memorized the directions of both the arrows. On execution trials, the baseline maze without the arrows reappeared, and the participants pressed buttons to indicate the directions of the two arrows (arrow on the left of the maze first). In the complex condition (cue "both"), the participants had to solve both arrow and maze tasks together. A maze with start and goal dots, blocks, and four arrows positioned within

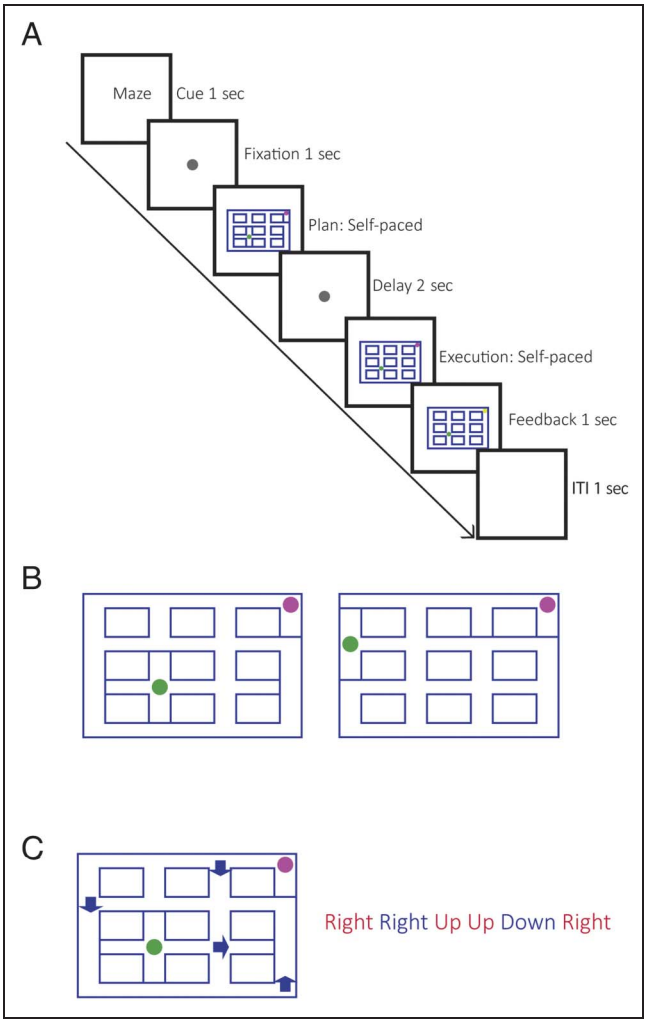

Figure 1. (A) The figure shows an example simple maze trial. The trial begins with a cue (1 sec), followed by a fixation period (1 sec) and then the planning phase. A blue maze is presented with green and magenta dots respectively indicating the starting position and goal. Blue lines extending across some paths indicate blocked paths. Participants press a button once they have planned a route from the start to the goal, avoiding the blocked paths. Following a delay of 2 sec, on 25% of the trials, there is an execution phase. The maze reappears with the start and the goal dots, but not the blocked paths. The participants execute their previously planned route and are given feedback for 1 sec. (B) Example planning phase mazes with start position in the center (left) or at the edge (right). Each maze was designed with only one open path adjacent to the start position and only one open path adjacent to the goal. All routes were four steps. Routes had one, two, or three turns. (C) Example maze from the complex condition (arrow and maze task to be done together). Start, goal, blocked paths, and arrows are present. The correct sequence of responses is shown to the right, with red indicating responses for the maze and blue indicating responses to arrows. Trials were only considered correct if all responses were made in the correct order.

the maze was presented (Figure 1C). Participants planned a route from the start to the goal, as they did in the simple maze condition, and at the same time remembered the direction of two arrows encountered along the route (but not the two others). Two other arrows were included so as to not bias the planning of the route toward where the arrows were. In the execution phase, participants pressed buttons to move from start to goal in the maze and, when the route reached an arrow, made an additional button press to indicate arrow direction (Figure 1C). The green dot only moved for responses that were part of the maze task route. In the time pressure condition (cue "fade"), the task was similar to the simple maze condition, but at the planning phase, the maze faded away into the white background over a period of 0.3–1.3 sec. The maze immediately started fading linearly from the moment it was presented. The fade time was fixed for each participant, as determined in a prescanning session (see Prescanning Session below). Note that, even though the maze faded, participants could still take as long as required to complete their plan and then pressed the button to proceed. Usually, this happened after the maze had fully disappeared. Finally, the reward condition (cue "fade + £1") was the same as the time pressure condition, except that, if the trial had an execution phase, a reward was given for correct completion (£1 per trial). The time pressure was present in the reward condition to make sure the participants did not study the maze longer to be more accurate.

In all conditions, execution trials were followed by a 1-sec feedback display. In the maze task, the goal circle turned yellow to indicate correct completion of the trial. A green tick indicated correct trials in the arrow task. In the maze task, an error was scored for a keypress not moving along an open path. In the arrow task, an error was scored for a keypress in the wrong direction. In the complex condition, these rules were combined, with the rule for the arrow task implemented whenever the sequence of responses reached an arrow position. Errors resulted in immediate termination of the trial and presentation of error feedback in the form of a red cross. A 1-sec intertrial interval separated consecutive trials.

Prescanning Session

A practice session took place before the scan. The participants carried out 25 simple maze trials, and two of each of the other conditions. Forty percent of the average planning time of the last 20 simple maze trials (excluding incorrect trials) was set as the fade time to be used in the scanner session. All trials in the prescanning session had an execution phase, and the participants were told that this was not always the case in the scanning session.

Scanning Session

The scanning session included a structural scan, an eye-tracking calibration, and two functional runs. Each run consisted of 192 trials, 32 trials of each of the six conditions, presented in a random order. Eight of the 32 were execution trials, except in the baseline condition, which had no execution phase. There were three breaks in each run. During this break, the money earned in the reward trials and the number of execution trials completed correctly were presented on the screen. The task resumed on a button press by the participants. The average ± *SD* EPI time for each run of the task was 24.8 ± 1.83 min. The task was written and presented using Psychtoolbox-3 (Brainard, 1997) and MATLAB (The MathWorks). Stimuli were projected on an MRI-compatible screen inside the scanner.

Data Acquisition

fMRI data were acquired using a Siemens 3T Prisma scanner with a 32-channel head coil. We used a multiband imaging sequence with a multiband factor of 3, acquiring 2-mm isotropic voxels (Feinberg et al., 2010). Other acquisition parameters were as follows: repetition time = 1.1 sec, echo time = 30 msec, 48 slices per volume with a slice thickness of 2 mm and no gap between slices, in plane resolution = 2 × 2 mm, field of view = 205 mm, and flip angle = 62°. T1-weighted multiecho MPRAGE (van der Kouwe, Benner, Salat, & Fischl, 2008) high-resolution images were also acquired for all participants (voxel size = 1 mm isotropic, field of view = 256 × 256 × 192 mm, repetition time = 2530 msec, echo time = 1.64, 3.5, 5.36, and 7.22 msec). The voxelwise root mean square across the four MPRAGE images was computed to obtain a single structural image.

Eye Tracking

The diameter and position of the participant's left pupil were continuously measured using an iView X Version 2.8.26 eye tracker (SensoMotoric Instruments [SMI], Teltow, Germany). A 9-point spatial calibration was performed before the task began. For each trial, the cue, fixation, planning, delay, execution, and intertrial interval phase onset markers were sent to the eye tracker from the MATLAB task script. The raw data obtained from the tracker were converted to a text file using SMI IDF Converter 3.0.15. For each participant, the mean pupil size during the planning phase was calculated for each trial and then averaged across all trials of the same condition. The BeGaze software from SMI was used to automatically detect fixation, blink, and saccade events. The number of saccades per second for the planning phase was calculated for each condition and participant.

fMRI Analysis

All analysis of fMRI data was performed using SPM12 (Wellcome Department of Imaging Neuroscience, London, United Kingdom; www.fil.ion.ucl.ac.uk) and the Automatic Analysis (aa) toolbox (Cusack et al., 2014). Initial processing included motion correction

and slice time correction. The structural image was coregistered to the Montreal Neurological Institute template, and then the mean EPI was coregistered to the structural image. The structural image was then normalized to the template via a nonlinear deformation, and the resulting transformation was applied on the EPI volumes. Spatial smoothing of a 5-mm FWHM was performed for whole-brain analyses only.

Separately for each of the six conditions, we created planning and execution regressors (planning only for the baseline condition), leaving cue, fixation, delay, and intertrial interval as part of the implicit baseline. For each of the four maze conditions (simple maze, complex, time pressure, and reward conditions), we separately modeled routes of one, two, and three turns from the central start position (see Figure 1B, left) and routes with one and two turns from the outer start position (see Figure 1B, right). The mean response to each maze condition was created by averaging these five separate route regressors. This was done to remove potential route effects, if any, from the condition contrasts presented in the analysis. Planning and execution phases were taken as lasting from stimulus onset to response (planning phase—button press indicating the end of planning; execution phase—final button press). To create regressors, measured durations for each phase on each trial were convolved with the canonical hemodynamic response function. Analyses concerned just regressors from the planning phase of each trial, with execution regressors, along with the six movement parameters and run means, included as covariates of no interest. Note that, for trials with an execution phase, planning data were included whether or not execution was correct.

Our primary analysis focused on a priori MD ROIs. For this analysis, we used a template for the MD network ROIs in Montreal Neurological Institute space as defined by Fedorenko et al. (2013; see *t* map at imaging.mrc-cbu.cam.ac.uk/imaging/MDsystem). Based on the regional divisions in the template, we selected the anterior, middle, and posterior parts of the middle frontal gyrus (aMFG, mMFG, and pMFG, respectively), pdLFC, AI/FO, preSMA/ACC, and IPS, symmetrically defined in the left and right hemispheres (Figure 4A). Using the MarsBaR toolbox (marsbar.sourceforge.net; Brett, Anton, Valabregue, & Poline, 2002) for SPM 12, beta estimates for each regressor of interest were averaged across runs and across voxels within each ROI, separately for each participant and condition. Contrasts between conditions were performed using *t* tests. To supplement ROI analysis, selected contrasts were also performed voxelwise across the whole brain, corrected for multiple comparisons using the false discovery rate, $p < .05$ (Benjamini & Hochberg, 1995).

In a supplementary analysis, we repeated critical contrasts in a set of more focused ROIs. Resting-state connectivity analyses often produce a "frontoparietal control" network resembling the MD network (Schaefer et al., 2018; Yeo et al., 2011). To isolate "frontoparietal control" voxels, we conjoined each of our MD ROIs with the corresponding frontoparietal control network from Yeo et al. (2011; seven-network parcellation). This conjunction produced regions of overlap in each of our a priori MD ROIs (minimum overlap 482 voxels, maximum 7965 voxels, separated by hemisphere). Analyses were then repeated on these reduced "conjunction" ROIs.

RESULTS

Behavior

RTs for the planning phase of each condition, along with accuracies for the execution phase, are shown in Table 1. All RTs were timed from display onset until response. In the baseline condition, it was display offset that triggered the response.

Planning RT was shortest in the baseline condition and longest in the complex condition, which required planning of responses for both tasks (simple maze and simple arrow). A repeated-measures ANOVA showed a main effect of Condition, $F(5, 23) = 87.59$, $p < .001$. A post hoc Tukey–Kramer multiple comparisons test showed that RTs in the baseline condition were significantly faster than all other conditions (all ps $< .001$). The complex condition had significantly longer RTs than all other conditions (all ps $< .001$). There was no RT difference between the simple arrow, simple maze, time pressure, and reward conditions (all ps $> .05$).

Accuracies of the execution trials were higher in the simple maze and simple arrow compared with the complex and reward (plus time pressure) conditions. A repeated-measures ANOVA showed a main effect of Condition, $F(4, 23) = 6.95$, $p < .001$. A post hoc Tukey–Kramer multiple comparisons test showed that accuracies in the complex condition were significantly lower than simple maze and simple arrow ($p < .01$ and $p < .02$, respectively). Accuracy rate for the reward (plus time pressure) condition was also lower than the simple maze and simple arrow conditions (both ps $< .02$). Accuracy in the time pressure condition was not significantly different from

Table 1. Planning Phase RTs and Execution Phase Accuracies in Each Condition

	Baseline	*Simple Maze*	*Simple Arrow*	*Complex*	*Time Pressure*	*Reward*
RT (sec)	1.11 ± 0.06	1.56 ± 0.08	1.53 ± 0.07	3.16 ± 0.20	1.58 ± 0.09	1.60 ± 0.09
Accuracy (% correct)		97.1 ± 0.75	96.6 ± 1.12	91.1 ± 1.68	91.9 ± 2.00	88.02 ± 2.41

Values are means ± standard errors.

any other condition ($p > .05$). The overall high execution accuracies and the unpredictability of the execution trials indicated that planning was indeed undertaken.

As noted above, maze routes differed in the number of turns required (one, two, or three), and imaging analyses were designed to remove these effects from comparisons between conditions. To examine the effect of the number of turns on planning time, we ran two-way repeated-measures ANOVA with Condition (simple maze, complex, time pressure, and reward) and Route complexity as factors (one, two, or three turns). The analysis showed a significant effect, $F(2, 46) = 15.45$, $p < .001$, with mean planning times for one-, two-, and three-turn routes of 1.94 ± 0.1 sec, 2.11 ± 0.1 sec, and 2.27 ± 0.1 sec, respectively. Post hoc tests with Tukey–Kramer multiple comparisons tests showed a shorter RT for the one-turn routes compared with both two-turn and three-turn routes (both ps $< .01$) and for two-turn routes compared with three-turn ($p < .01$).

Imaging

Imaging analyses concerned just the planning phase of each trial. For each ROI, contrasts of the five active tasks against baseline are shown in Figure 2. Note that results for each ROI are averaged over left and right hemispheres, with ROIs illustrated on the left hemisphere in the center panel. Separate results for the two hemispheres are shown in Supplementary Figure S1.[1]

The most striking difference between ROIs concerned the contrast of simple tasks against baseline. In both hemispheres, this contrast was significant in IPS, pdLFC, preSMA/ACC, and pMFG, with little hint of activation for remaining ROIs. The same remained true in the complex condition,

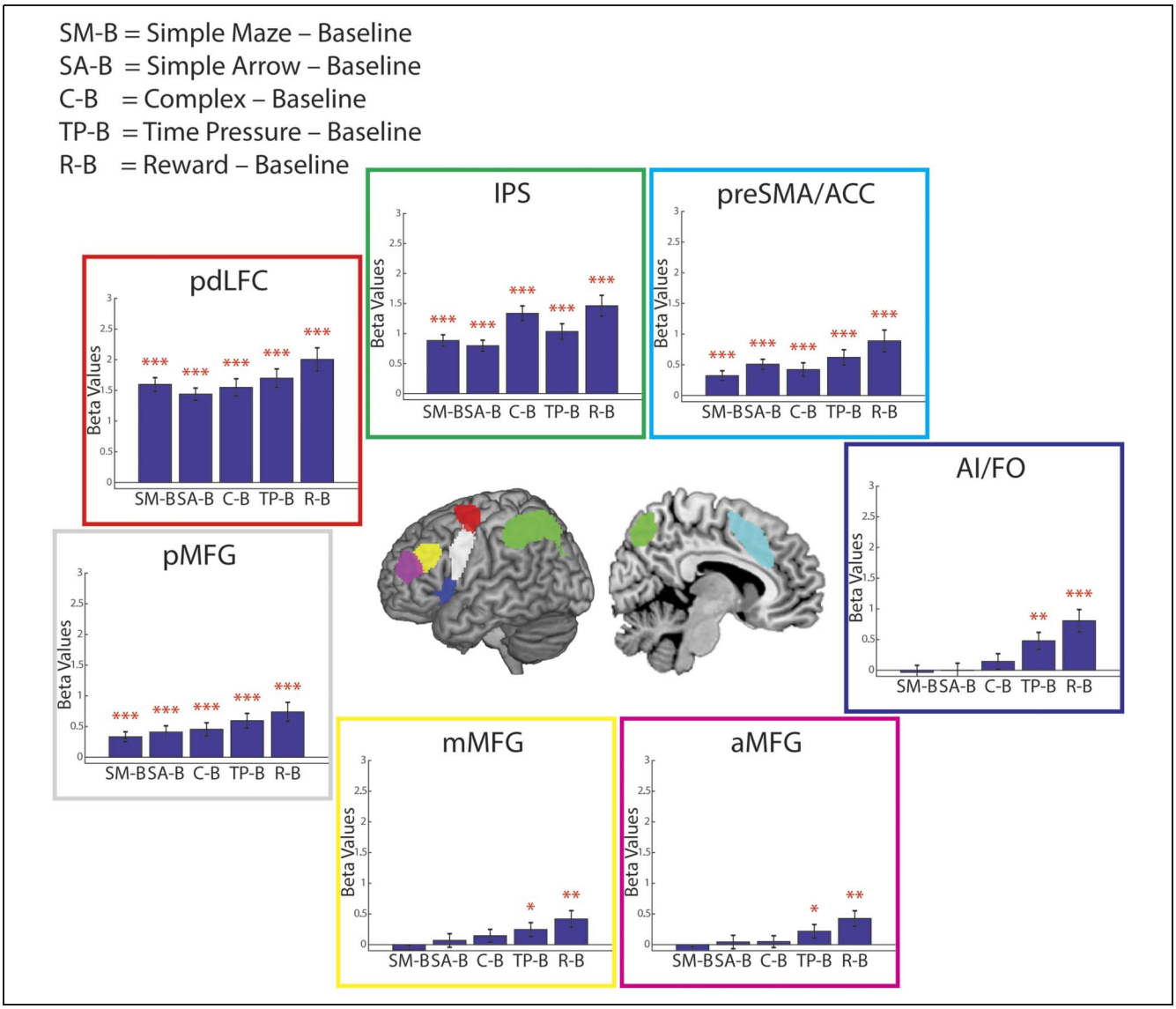

Figure 2. Separate panels for each ROI show contrasts (beta values) for each condition minus the baseline condition, with *SEM*. Red asterisks show significance for a one-tailed t test against zero (*$p < .05$, **$p < .01$, ***$p < .001$). Results are averaged across hemispheres, with ROIs (center panel) illustrated on the left hemisphere.

though the contrast with baseline was now numerically positive in all ROIs of both hemispheres. With time pressure, significant activity against baseline extended to include all ROIs. This activity in all ROIs was further strengthened in the reward condition.

To provide an initial statistical overview, we entered these contrasts against baseline into a three-way repeated-measures ANOVA with factors Condition (5), ROI (7), and Hemisphere (2). The analysis showed a significant main effect of Condition, $F(4, 92) = 13.43$, $p < .001$, reflecting the generally increasing pattern of activity from left to right within each panel of Figure 2. There was also a main effect of ROI, $F(6, 138) = 77.64$, $p < .001$, indicating much stronger overall activation for some ROIs (especially pdLFC and IPS) than others (especially AI/FO, mMFG, and aMFG). Though activations were broadly similar on the two sides (Supplementary Figure S1), there was also a significant main effect of Hemisphere, $F(1, 23) = 25.44$, $p < .001$. Finally, there were interactions between Condition and ROI, $F(24, 552) = 10.03$, $p < .001$; Condition and Hemisphere, $F(4, 92) = 26.93$, $p < .001$; ROI and Hemisphere, $F(6, 138) = 4.68$, $p < .001$; and between Condition, ROI, and Hemisphere, $F(24, 552) = 8.05$, $p < .001$, all indicating a degree of functional differentiation between ROIs.

Specific contrasts were then used to isolate the effects of individual variables (Figure 3). Again, results were broadly similar in left and right hemispheres, though with some quantitative differences (see Supplementary Figure S2). In the following sections, we report significant effects averaged across hemispheres, accompanied by results of an ANOVA separating the two.

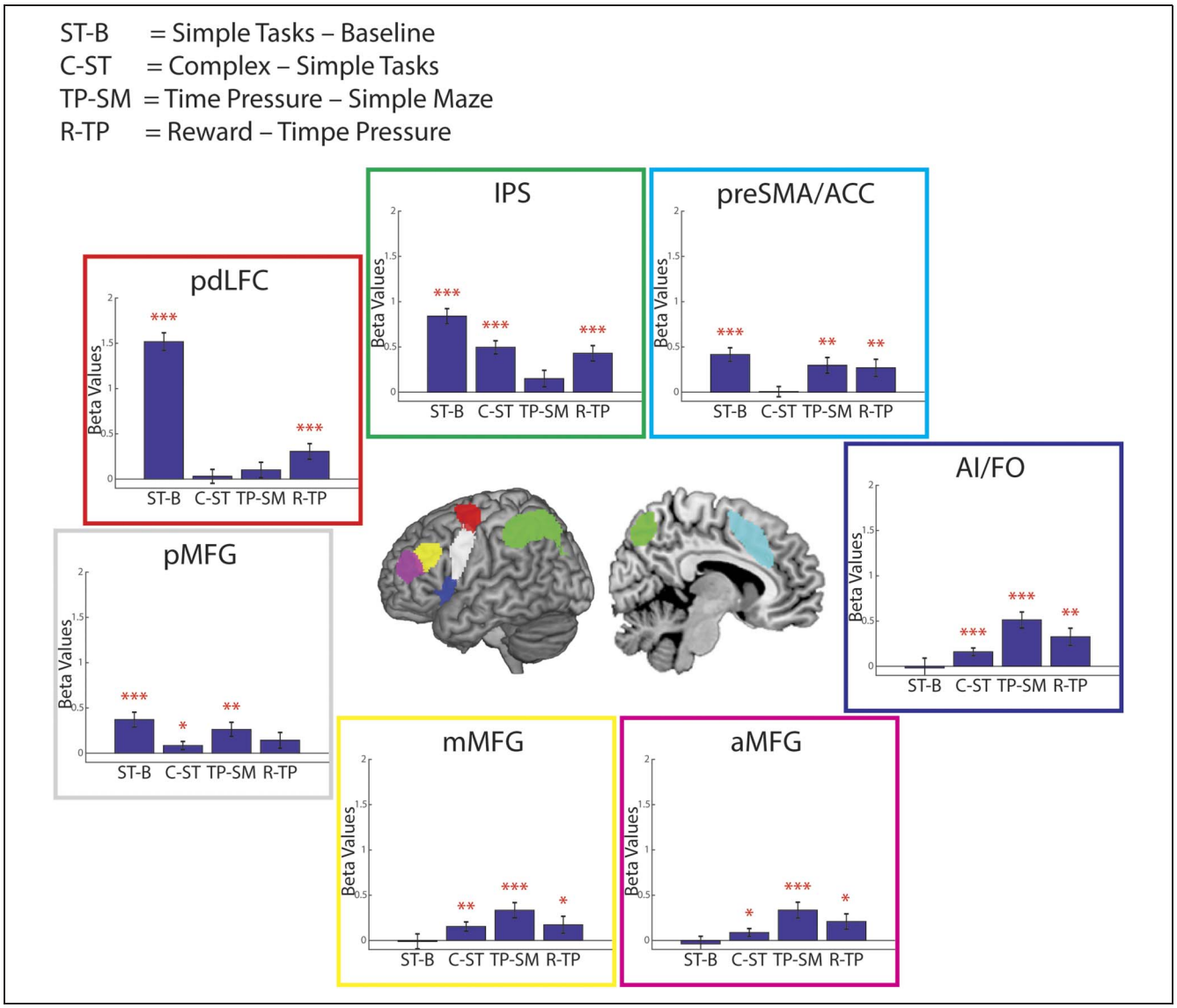

Figure 3. Separate panels for each ROI show effects (beta values) for each contrast: average of simple tasks versus baseline, complex versus average of simple tasks, time pressure versus simple maze, and reward versus time pressure; with *SEM*. Red asterisks show significance for a one-tailed *t* test against zero (*$p < .05$, **$p < .01$, ***$p < .001$). Results are averaged across hemispheres, with ROIs (center panel) illustrated on the left.

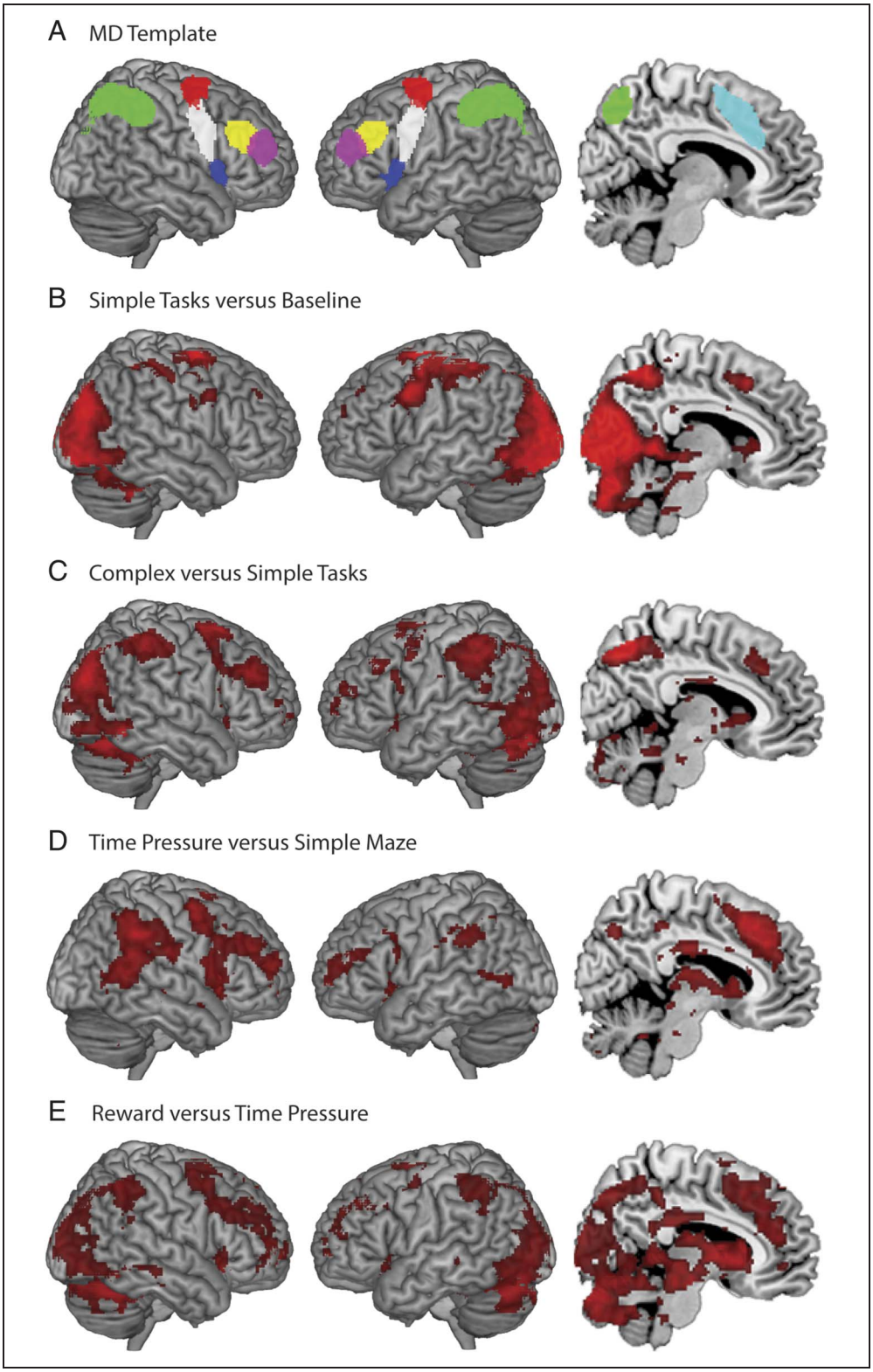

Figure 4. Whole-brain contrasts. (A) Templates of the MD system used for the ROI analysis. (B–E) *t* Statistics associated with significant contrasts of (B) average of simple tasks versus baseline, (C) complex versus average of simple tasks, (D) time pressure versus simple maze, and (E) reward versus time pressure. Contrasts are corrected for multiple comparisons using false discovery rate ($p < .05$). Maps do not include activity in the dorsal part of the parietal lobe, as data for this region were not acquired for four participants. Note that ROI results do not change on excluding those four participants.

Simple Tasks versus Baseline

To examine brain activity associated with the simplest versions of our tasks, we used a contrast of simple tasks (mean of simple maze and simple arrow) against baseline. In Figure 3, results for each MD ROI are shown in the leftmost column of each panel. For this contrast, there was significant univariate activity in only a part of the MD network and, in particular, within LFC, only for the most posterior regions. The contrast was significant for pdLFC, $t(23) = 15.50$, $p < .001$, $d = 2.55$; pMFG, $t(23) = 4.49$, $p < .001$, $d = 0.84$; preSMA/ACC, $t(23) = 5.60$, $p < .001$, $d = 0.81$; and IPS,

$t(23) = 10.06, p < .001, d = 1.44$, but with little hint of activity in AI/FO, mMFG, or aMFG ($p > .1$ for all).

A repeated-measures ANOVA for this contrast had factors ROI (7) and Hemisphere (2). Confirming this selectivity, there was a highly significant main effect of ROI, $F(6, 23) = 84.01, p < .001$. In addition, the analysis showed main effects of Hemisphere, $F(1, 23) = 48.66, p < .001$, and an interaction between the two, $F(6, 23) = 7.02, p < .001$. Though the main pattern of results was generally similar on the two sides (Supplementary Figure S2), only the left hemisphere showed significant activity in the pMFG.

A complementary whole-brain analysis for this contrast (Figure 4B) confirmed the above picture, with activity significant in posterior dorsal LFC, parietal cortex, and preSMA, accompanied by the expected substantial recruitment of visual areas.

Complexity

A contrast of the complex condition versus the mean of the two simple tasks was used to examine effects of complexity. Results for each MD ROI are shown in the second column of each panel in Figure 3. In IPS and pMFG, activity already present in the simple tasks was further increased in the complex condition, especially in IPS ($t(23) = 6.92, p < .001, d = 1.14$ for IPS and $t(23) = 1.84, p = .039, d = 0.22$ for pMFG). With increasing complexity, activity also appeared in three new MD regions, AI/FO, $t(23) = 3.71, p < .001, d = 0.49$; mMFG, $t(23) = 3.09, p < .01, d = 0.38$; and aMFG, $t(23) = 2.00, p < .05, d = 0.21$. pMFG showed significant activity only in the left hemisphere, whereas mMFG and aMFG showed activity only in the right (Supplementary Figure S2). For pdLFC and preSMA/ACC, activity already present in the simple tasks remained at the same level in the complex condition ($p > .1$ for both), though this conclusion is tempered by whole-brain analysis (see below).

A repeated-measures ANOVA for this contrast showed a main effect of ROI, $F(6, 23) = 20.96, p < .001$, an interaction of ROI and Hemisphere, $F(6, 23) = 2.77, p < .05$, but no main effect of Hemisphere. Again, the pattern of results was broadly similar on the two sides, with the differences noted above for pMFG, mMFG, and aMFG (Supplementary Figure S2).

For this contrast, whole-brain analysis (Figure 4C) showed increased activity throughout the MD network, including regions that were and were not activated by the simple tasks alone. A small region of significant increase was observed in the preSMA/ACC, though not sufficient (and/or too anterior) to determine results in the entire ROI. Similarly, in the posterior dorsal frontal cortex, whole-brain analysis suggested additional activity in the complex condition, but immediately anterior to the a priori pdLFC ROI.

Time Pressure

Figure 3 shows results for the time pressure manipulation in the third column of each panel. Most MD regions showed increased activity with increasing time pressure: $t(23) = 5.82, p < .001, d = 1.26$ for AI; $t(23) = 3.84, p < .001, d = 0.74$ for aMFG; $t(23) = 3.94, p < .001, d = 0.67$ for mMFG; $t(23) = 3.35, p < .01, d = 0.59$ for pMFG; and $t(23) = 3.45, p < .01, d = 0.65$ for preSMA/ACC. The exceptions were pdLFC and IPS that did not show this effect ($p > .05$ in each case), though for IPS, the effect was significant in the right hemisphere (Supplementary Figure S1). With time pressure, in particular, aMFG was now strongly added to the active network.

Repeated-measures ANOVA for this contrast showed a main effect of ROI, $F(6, 23) = 9.44, p < .001$; a main effect of Hemisphere, $F(1, 23) = 5.15, p < .05$; and an interaction between the two, $F(6, 23) = 3.09, p < .05$.

The corresponding whole-brain map (Figure 4D) confirmed this picture, with activity now extending into anterior regions of MFG and AI. Whole-brain maps again showed increased activity in a region immediately anterior to the pdLFC ROI. Additional bilateral activity was seen in posterior temporal cortex.

Reward

To isolate the effect of potential reward, we contrasted the "reward" condition with the "time pressure" condition. These conditions had matched time pressure and differed only in whether correct performance was rewarded. In Figure 3, results for this contrast are shown in the rightmost column of each panel. Significant increases with reward appeared in all ROIs except pMFG ($t(23) = 3.43, p < .01, d = 0.61$ for AI; $t(23) = 2.46, p < .02, d = 0.43$ for aMFG; $t(23) = 1.84, p < .05, d = 0.35$ for mMFG; $t(23) = 2.82, p < .01, d = 0.43$ for preSMA/ACC; $t(23) = 5.05, p < .001, d = 0.80$ for IPS; and $t(23) = 3.50, p < .001, d = 0.42$ for pdLFC; for pMFG, $p = .056, d = 0.26$).

Repeated-measures ANOVA for this contrast showed a main effect of ROI, $F(6, 23) = 8.18, p < .001$, but not of Hemisphere. There was also a significant interaction, $F(6, 23) = 4.33, p < .05$. In all three MFG regions, reward effects were significant on the right but not in the left (Supplementary Figure S2).

The corresponding whole-brain map (Figure 4E) confirmed this picture, with the map showing the entire MD network, especially in the right hemisphere. Again, there was a further activity increase immediately anterior to the a priori pdLFC ROI. Increased activity was also seen in more rostral parts of ACC, along with visual cortex and multiple subcortical structures including ventral and dorsal striatum, in line with well-known roles in reward processing.

Conjunction ROIs

In a supplementary analysis, contrasts were repeated for reduced ROIs, formed by the intersection of our MD ROIs with a frontoparietal control network from Yeo et al.

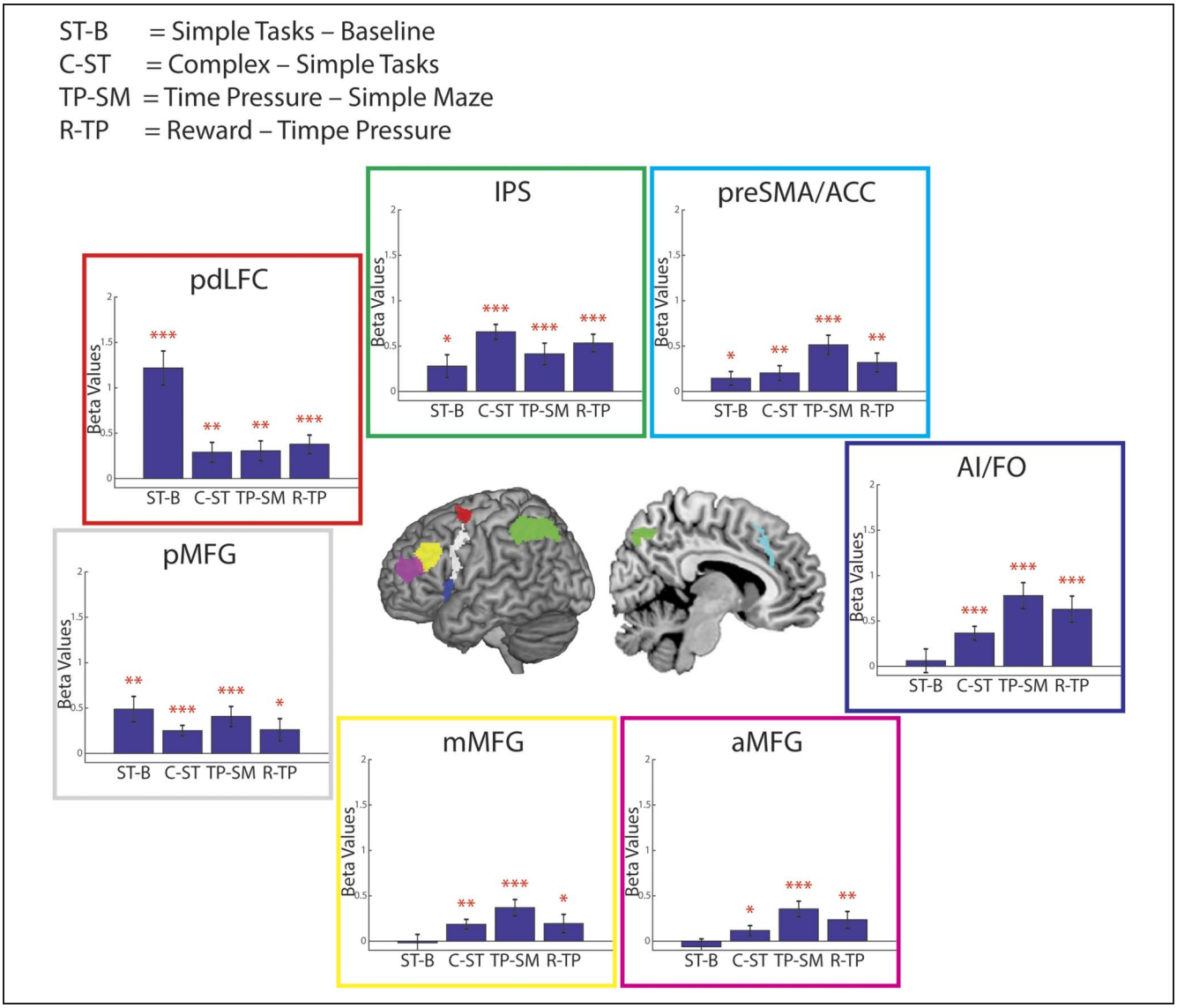

Figure 5. Data as in Figure 3 for reduced ROIs (overlap of a priori MD ROIs with frontoparietal control network from Yeo et al., 2011). Reduced ROIs (center panel) are illustrated on the left hemisphere.

(2011). Results are shown in Figure 5. Again, only IPS, pdLFC, pMFG, and preSMA/ACC were more active in the simple tasks compared with the baseline. Using these more focused ROIs, all regions showed increased activity in the complex contrast, including pdLFC and preSMA/ACC, which did not show this effect when the entire ROI was used. All regions also showed significant effects of time pressure (previously absent in pdLFC and IPS) and reward (previously absent in pMFG). With these more focused ROIs, there was a clarified picture of selective activity in simple tasks, coupled with increasing activity across the entire network with increase in complexity, time pressure, and reward.

Eye Tracking

For each condition, Table 2 shows the mean increase in pupil size between the initial fixation phase of each trial (1 sec following the task cue; see Figure 1) and the planning phase. A one-way repeated-measures ANOVA showed a main effect of Condition, $F(5, 23) = 10.62$, $p < .001$. A post hoc Tukey–Kramer multiple comparisons test showed that pupil dilation in the reward condition was higher than all other conditions ($p < .005$ for comparison with all other conditions, $d = 1.12, 1.36, 1.28, 1.46$, and 0.56 for baseline, simple maze, simple arrow, complex, and time pressure, respectively). No other differences were significant, though a planned comparison between the time pressure and simple maze conditions showed a trend in the predicted direction, $t(23) = 1.84$, $p = .074$. Pupil sizes during the initial fixation period were not significantly different between conditions.

Saccade rates (number of saccades per second) for each condition are also shown in Table 2. A one-way repeated-measures ANOVA showed a main effect of

Table 2. Planning Phase: Pupil Size (Increase from Fixation Period) and Saccade Rate

	Baseline	*Simple Maze*	*Simple Arrow*	*Complex*	*Time Pressure*	*Reward*
Size increase (mm)	0.10 ± 0.07	0.11 ± 0.05	0.07 ± 0.04	0.06 ± 0.03	0.27 ± 0.11	0.55 ± 0.11
Saccade rate (saccades/sec)	2.57 ± 0.14	3.20 ± 0.15	3.43 ± 0.15	3.31 ± 0.14	2.93 ± 0.16	3.01 ± 0.12

Values are means ± standard errors.

Condition, $F(5, 23) = 15.10$, $p < .001$. Similar post hoc tests as for pupil size analysis showed that the baseline condition had the lowest saccade rate ($p < .001$, $d = 1.34$ and $d = 1.11$ for comparison with simple maze and complex; $p < .05$, $d = 0.91$ and $d = 0.72$ with simple arrow and reward; and $p = .13$, $d = 0.50$ with time pressure). Saccade rates were higher in the simple maze condition compared with time pressure and reward ($p < .001$, $d = 0.67$ and $d = 0.65$), probably because, in the latter, the maze disappeared while planning was still in progress. Saccade rates were similar in simple maze, simple arrow, and complex conditions ($p > .1$).

DISCUSSION

MD regions are recruited in many different cognitive tasks. Previously, we have suggested that they construct the successive steps of a mental control program, each step binding together the required stimuli, responses, and rules into the correct combinations. Across MD regions, previous data suggest a degree of specialization especially at low load, with progressive recruitment of the entire network as load increases. While differentiation between MD regions may reflect preferential access to different task features, co-recruitment may reflect increasing information integration and exchange—matching the findings of multivoxel pattern analysis with widespread but quantitatively varying representation of multiple task features across MD regions (Woolgar et al., 2016). To examine differentiation and co-recruitment, we used a spatial maze and manipulations of complexity, time pressure, and reward, comparing profiles of activity across an a priori set of MD regions.

As predicted, the strongest differentiation between MD regions came from the comparison of simple tasks against baseline. For this contrast, the results suggested recruitment of a largely posterior frontal network, including pdLFC and pMFG, accompanied by IPS and preSMA/ACC (Figure 3). The MD regions examined here show increased activity in many tasks, some with no evident spatial element (Fedorenko et al., 2013). At the same time, as noted earlier, it is likely that regions overlapping with or close to pdLFC and IPS have strong involvement in spatial operations, and indeed, much imaging evidence indicates a relative specialization of these regions for spatial tasks (Nee et al., 2013; Rottschy et al., 2012; Owen, McMillan, Laird, & Bullmore, 2005; Wager & Smith, 2003). With close proximity and functional connections to other spatial regions, pdLFC and IPS may be the first to be strongly recruited in a spatial task, with additional MD regions added as demands increase. Beyond this specific role in spatial operations, it is also possible that posterior frontal and parietal regions are the first to be recruited in many kinds of task, with activity spreading anteriorly as demands increase. This would match previous results suggesting anterior spread with increased rule complexity (e.g., Crittenden & Duncan, 2014; Badre & D'Esposito, 2007, 2009). More work is needed to establish whether the current results are specific to tasks with a strong spatial element or whether they are more general and apply to other cognitive domains as well.

In the complex condition, as predicted, there was widespread increase of activity across the MD network. This increase was especially clear in the reduced ROIs produced by overlapping our a priori MD regions with the Yeo et al. (2011) frontoparietal control network (Figure 5). As compared with simple tasks, activity now spread forward along the lateral frontal surface and appeared in AI/FO. Of those regions already recruited in the simple tasks, activity further increased in IPS and pMFG, though for pdLFC and preSMA/ACC, this was visible only in the reduced ROIs.

Time pressure was introduced to make the simple maze task more challenging, while keeping computational operations much the same. Based on the literature, we thought it possible that AI/FO and preSMA/ACC would be the most sensitive to time pressure, and indeed, the effect was numerically strongest in AI/FO. More broadly, however, the pattern of results resembled the effects of complexity, with strengthened activity in several of those regions already involved in the simple tasks (pMFG, right IPS, and preSMA/ACC), maintained activity in others (pdLFC), and now strong recruitment of all remaining MD regions (AI/FO, mMFG, and aMFG). Again, increases were more consistent in reduced ROIs formed from overlap with the Yeo et al. (2011) frontoparietal control network. In line with these findings, other studies have implicated bilateral LFC, ACC, and AI in processing speeded stimuli (Loose, Kaufmann, Tucha, Auer, & Lange, 2006; Peelle, McMillan, Moore, Grossman, & Wingfield, 2004).

Similarly, we had anticipated that selected MD regions—especially preSMA/ACC—might be most sensitive to reward, but instead, reward effects were widespread throughout the MD network. The whole brain

contrast in the reward condition also showed activation in subcortical regions—including ventral and dorsal striatum, both involved in reward processing (Clithero & Rangel, 2014; Bartra, McGuire, & Kable, 2013; Liu, Hospadaruk, Zhu, & Gardner, 2011)—and spreading forward from preSMA/ACC into reward-related rostral ACC (de la Vega, Chang, Banich, Wager, & Yarkoni, 2016). Another notable feature of the whole-brain map—shared with the time pressure condition—was activity around the TPJ. Activity in this region has often been associated with unusual, important events (Krall et al., 2015; Downar, Crawley, Mikulis, & Davis, 2002), perhaps including the challenge that was introduced with the disappearance of the maze to be solved. Widespread MD recruitment with increasing reward is broadly consistent with a number of previous studies (Dixon & Christoff, 2012; Padmala & Pessoa, 2011).

Regarding pupil size, we found a significant increase over baseline only in the reward condition, with some additional evidence for the predicted increase in the time pressure condition. Our results are consistent with those of Chiew and Braver (2014), Gergelyfi et al. (2015), and Muhammed et al. (2016), who all found pupil size to be correlated with reward magnitude. Greatest pupil dilation in the reward condition was associated with strongest response throughout the MD system (Figure 2).

Though our three manipulations all showed a broad pattern of MD co-recruitment, there were also clear quantitative differences between ROIs. For each manipulation, ANOVA showed significant effects of ROI, with additional differences in exact activity pattern between hemispheres. For complexity, for example, the strongest effect was seen in the IPS. Plausibly, the IPS has most immediate access to the spatial features of the task and thus most sensitive to the increases spatial demand of interleaving maze and arrow processing. For time pressure, in contrast, the strongest effect was seen in AI/FO, accompanied by the trend to increased pupil dilation mentioned above. Among MD regions, perhaps AI/FO, as we had predicted, is most closely associated with autonomic arousal, showing the dominant response as arousal increases. At the same time, effective cognition requires multiple task features to be integrated. For example, when time pressure and reward drive autonomic arousal and mental effort, this effort must be specifically linked to the spatial operations of maze and arrow processing. Such integration, we suggest, is reflected in broad MD co-recruitment for all task manipulations.

An important question is the potential contribution of eye movements to our results. Plausibly, in particular, both pdLFC and IPS might contribute to control and production of saccades, with pdLFC lying close to the location of the human FEF (Corbetta et al., 1998; Pierrot-Deseilligny et al., 1991) and the IPS containing the parietal eye field (Muri, Vermersch, Rivaud, Gaymard, & Pierrot-Deseilligny, 1996). Saccades of course were more frequent in all active conditions compared with baseline, somewhat resembling the activity profile of pdLFC. It seems unlikely, however, that activity profiles in IPS and perhaps also pdLFC can be entirely explained by overt saccadic activity. For example, the rate of saccade production was well matched in complex and simple tasks, whereas complexity strongly increased IPS activity. Saccades may well have contributed, however, especially to activity in pdLFC, along with possible differences in planning of both executed and nonexecuted saccades.

In this light, it is intriguing that, in whole-brain analysis, we found increased activity linked to complexity and time pressure in a region just anterior to our pdLFC ROI. In recent analysis of data from the Human Connectome Project, we have found evidence for an MD region lying not in the human FEF, but just anterior to it (Assem, Glasser, Van Essen, & Duncan, 2019). Given individual variability between participants and uncertainties in coregistration, it is possible that, in the current study, the pdLFC ROI derived from previous data was dominated, not by the intended MD region, but by FEF lying just posterior to it. Higher spatial-resolution fMRI data could be used to address this possibility.

Across the MD system, our results illustrate the balance between relative specialization, especially at low load, and progressive co-recruitment as demand or motivation increases. Across MD regions, there were clear quantitative differences in response to our three manipulations of complexity, time pressure, and reward. At the same time, the broad pattern of progressive MD recruitment was much the same across manipulations. At each step of a mental control program, different kinds of mental content must be integrated to produce the required cognitive operations. Especially at low load, differentiation between MD regions may reflect preferential access to different task features. As task demands or motivation increases, however, there is increasing information exchange and integration, reflected in increasingly widespread activity across the MD network.

Acknowledgments

This work was funded by the Medical Research Council (United Kingdom) Intramural Program MC-A060-5PQ10. Sneha Shashidhara was supported by a scholarship from the Gates Cambridge Trust, Cambridge, UK. Yaara Erez was supported by a Royal Society Dorothy Hodgkin Research Fellowship, UK (DH130100).

Reprint requests should be sent to Sneha Shashidhara, MRC Cognition and Brain Sciences Unit, 15 Chaucer Road, Cambridge CB2 7EF, United Kingdom, or via e-mail: sneha.shashidhara@mrc-cbu.cam.ac.uk.

Note

1. Supplementary material can be retrieved from the following: Supplementary Figure S1 (10.6084/m9.figshare.8870071), Supplementary Figure S2 (10.6084/m9.figshare.8870065).

REFERENCES

Alnaes, D., Sneve, M. H., Espeseth, T., Endestad, T., van de Pavert, S. H., & Laeng, B. (2014). Pupil size signals mental effort deployed during multiple object tracking and predicts brain activity in the dorsal attention network and the locus coeruleus. *Journal of Vision*, *14*, 1.

Assem, M., Glasser, M. F., Van Essen, D. C., & Duncan, J. (2019). A domain-general cognitive core defined in multimodally parcellated human cortex. *BioRxiv*, 517599. https://doi.org/10.1101/517599.

Badre, D. (2008). Cognitive control, hierarchy, and the rostro-caudal organization of the frontal lobes. *Trends in Cognitive Sciences*, *12*, 193–200.

Badre, D., & D'Esposito, M. (2007). Functional magnetic resonance imaging evidence for a hierarchical organization of the prefrontal cortex. *Journal of Cognitive Neuroscience*, *19*, 2082–2099.

Badre, D., & D'Esposito, M. (2009). Is the rostro-caudal axis of the frontal lobe hierarchical? *Nature Reviews Neuroscience*, *10*, 659–669.

Badre, D., & Nee, D. E. (2018). Frontal cortex and the hierarchical control of behavior. *Trends in Cognitive Sciences*, *22*, 170–188.

Bartra, O., McGuire, J. T., & Kable, J. W. (2013). The valuation system: A coordinate-based meta-analysis of BOLD fMRI experiments examining neural correlates of subjective value. *Neuroimage*, *76*, 412–427.

Benjamini, Y., & Hochberg, Y. (1995). Controlling the false discovery rate: A practical and powerful approach to multiple testing. *Journal of the Royal Statistical Society. Series B (Methodological)*, *57*, 289–300.

Botvinick, M., & Braver, T. (2015). Motivation and cognitive control: From behavior to neural mechanism. *Annual Review of Psychology*, *66*, 80–113.

Brainard, D. H. (1997). The psychophysics toolbox. *Spatial Vision*, *10*, 433–436.

Brett, M., Anton, J.-L., Valabregue, R., & Poline, J.-B. (2002). Region of interest analysis using an SPM toolbox [abstract]. Presented at the 8th International Conference on Functional Mapping of the Human Brain, June 2–6, 2002, Sendai, Japan. Available on CD-ROM in NeuroImage, Vol. 16, No. 2, abstract 497.

Camilleri, J. A., Müller, V. I., Fox, P., Laird, A. R., Hoffstaedter, F., Kalenscher, T., et al. (2018). Definition and characterization of an extended multiple-demand network. *Neuroimage*, *165*, 138–147.

Chiew, K. S., & Braver, T. S. (2014). Dissociable influences of reward motivation and positive emotion on cognitive control. *Cognitive, Affective and Behavioral Neuroscience*, *14*, 509–529.

Clithero, J. A., & Rangel, A. (2014). Informatic parcellation of the network involved in the computation of subjective value. *Social Cognitive and Affective Neuroscience*, *9*, 1289–1302.

Cole, M. W., Ito, T., & Braver, T. S. (2016). The behavioral relevance of task information in human prefrontal cortex. *Cerebral Cortex*, *26*, 2497–2505.

Corbetta, M., Akbudak, E., Conturo, T. E., Snyder, A. Z., Ollinger, J. M., Drury, H. A., et al. (1998). A common network of functional areas for attention and eye movements. *Neuron*, *21*, 761–773.

Critchley, H. D., Mathias, C. J., Josephs, O., O'Doherty, J., Zanini, S., Dewar, B. K., et al. (2003). Human cingulate cortex and autonomic control: Converging neuroimaging and clinical evidence. *Brain*, *126*, 2139–2152.

Critchley, H. D., Wiens, S., Rotshtein, P., Öhman, A., & Dolan, R. J. (2004). Neural systems supporting interoceptive awareness. *Nature Neuroscience*, *7*, 189–195.

Crittenden, B. M., & Duncan, J. (2014). Task difficulty manipulation reveals multiple demand activity but no frontal lobe hierarchy. *Cerebral Cortex*, *24*, 532–540.

Crittenden, B. M., Mitchell, D. J., & Duncan, J. (2016). Task encoding across the multiple demand cortex is consistent with a frontoparietal and cingulo-opercular dual networks distinction. *Journal of Neuroscience*, *36*, 6147–6155.

Cusack, R., Vicente-Grabovetsky, A., Mitchell, D. J., Wild, C. J., Auer, T., Linke, A. C., et al. (2014). Automatic Analysis (aa): Efficient neuroimaging workflows and parallel processing using MATLAB and XML. *Frontiers in Neuroinformatics*, *8*, 90.

de la Vega, A., Chang, L. J., Banich, M. T., Wager, T. D., & Yarkoni, T. (2016). Large-scale meta-analysis of human medial frontal cortex reveals tripartite functional organization. *Journal of Neuroscience*, *36*, 6553–6562.

Dixon, M. L., & Christoff, K. (2012). The decision to engage cognitive control is driven by expected reward-value: Neural and behavioral evidence. *PLOS ONE*, *7*, e51637.

Dosenbach, N. U., Fair, D. A., Miezin, F. M., Cohen, A. L., Wenger, K. K., Dosenbach, R. A., et al. (2007). Distinct brain networks for adaptive and stable task control in humans. *Proceedings of the National Academy of Sciences, U.S.A.*, *104*, 11073–11078.

Downar, J., Crawley, A. P., Mikulis, D. J., & Davis, K. D. (2002). A cortical network sensitive to stimulus salience in a neutral behavioral context across multiple sensory modalities. *Journal of Neurophysiology*, *87*, 615–620.

Duncan, J. (2001). An adaptive coding model of neural function in prefrontal cortex. *Nature Reviews Neuroscience*, *2*, 820–829.

Duncan, J. (2006). EPS mid-career award 2004: Brain mechanisms of attention. *Quarterly Journal of Experimental Psychology*, *59*, 2–27.

Duncan, J. (2010). The multiple-demand (MD) system of the primate brain: Mental programs for intelligent behaviour. *Trends in Cognitive Sciences*, *14*, 172–179.

Duncan, J. (2013). The structure of cognition: Attentional episodes in mind and brain. *Neuron*, *80*, 35–50.

Duncan, J., & Owen, A. M. (2000). Common regions of the human frontal lobe recruited by diverse cognitive demands. *Trends in Neurosciences*, *23*, 475–483.

Fedorenko, E., Duncan, J., & Kanwisher, N. (2013). Broad domain generality in focal regions of frontal and parietal cortex. *Proceedings of the National Academy of Sciences, U.S.A.*, *110*, 16616–16621.

Feinberg, D. A., Moeller, S., Smith, S. M., Auerbach, E., Ramanna, S., Gunther, M., et al. (2010). Multiplexed echo planar imaging for sub-second whole brain fMRI and fast diffusion imaging. *PLOS ONE*, *5*, e15710.

Gergelyfi, M., Jacob, B., Olivier, E., & Zénon, A. (2015). Dissociation between mental fatigue and motivational state during prolonged mental activity. *Frontiers in Behavioral Neuroscience*, *9*, 176.

Hadland, K. A., Rushworth, M. F., Gaffan, D., & Passingham, R. E. (2003). The anterior cingulate and reward-guided selection of actions. *Journal of Neurophysiology*, *89*, 1161–1164.

Hampshire, A., Highfield, R. R., Parkin, B. L., & Owen, A. M. (2012). Fractionating human intelligence. *Neuron*, *76*, 1225–1237.

Hampshire, A., Thompson, R., Duncan, J., & Owen, A. M. (2011). Lateral prefrontal cortex subregions make dissociable contributions during fluid reasoning. *Cerebral Cortex*, *21*, 1–10.

Kennerley, S. W., & Wallis, J. D. (2009). Reward-dependent modulation of working memory in lateral prefrontal cortex. *Journal of Neuroscience*, *29*, 3259–3270.

Knutson, B., Taylor, J., Kaufman, M., Peterson, R., & Glover, G. (2005). Distributed neural representation of expected value. *Journal of Neuroscience*, *25*, 4806–4812.
Krall, S. C., Rottschy, C., Oberwelland, E., Bzdok, D., Fox, P. T., Eickhoff, S. B., et al. (2015). The role of the right temporoparietal junction in attention and social interaction as revealed by ALE meta-analysis. *Brain Structure and Function*, *220*, 587–604.
Liu, T., Hospadaruk, L., Zhu, D. C., & Gardner, J. L. (2011). Feature-specific attentional priority signals in human cortex. *Journal of Neuroscience*, *31*, 4484–4495.
Loose, R., Kaufmann, C., Tucha, O., Auer, D. P., & Lange, K. W. (2006). Neural networks of response shifting: Influence of task speed and stimulus material. *Brain Research*, *1090*, 146–155.
Matsumoto, K., Suzuki, W., & Tanaka, K. (2015). Neuronal correlates of goal-based motor selection in the prefrontal cortex. *Science*, *301*, 229–232.
Muhammed, K., Manohar, S., Ben Yehuda, M., Chong, T. T.-J., Tofaris, G., Lennox, G., et al. (2016). Reward sensitivity deficits modulated by dopamine are associated with apathy in Parkinson's disease. *Brain*, *139*, 2706–2721.
Muri, R. M., Vermersch, A. I., Rivaud, S., Gaymard, B., & Pierrot-Deseilligny, C. (1996). Effects of single-pulse transcranial magnetic stimulation over the prefrontal and posterior parietal cortices during memory-guided saccades in humans. *Journal of Neurophysiology*, *76*, 2102–2106.
Murphy, P. R., Boonstra, E., & Nieuwenhuis, S. (2016). Global gain modulation generates time-dependent urgency during perceptual choice in humans. *Nature Communications*, *7*, 13526.
Nee, D. E., Brown, J. W., Askren, M. K., Berman, M. G., Demiralp, E., Krawitz, A., et al. (2013). A meta-analysis of executive components of working memory. *Cerebral Cortex*, *23*, 264–282.
Nomura, E. M., Gratton, C., Visser, R. M., Kayser, A., Perez, F., & D'Esposito, M. (2010). Double dissociation of two cognitive control networks in patients with focal brain lesions. *Proceedings of the National Academy of Sciences, U.S.A.*, *107*, 12017–12022.
Nyberg, L., Marklund, P., Persson, J., Cabeza, R., Forkstam, C., Petersson, K. M., et al. (2003). Common prefrontal activations during working memory, episodic memory, and semantic memory. *Neuropsychologia*, *41*, 371–377.
Owen, A. M. (1997). The functional organization of working memory processes within human lateral frontal cortex: The contribution of functional neuroimaging. *European Journal of Neuroscience*, *9*, 1329–1339.
Owen, A. M., McMillan, K. M., Laird, A. R., & Bullmore, E. (2005). N-back working memory paradigm: A meta-analysis of normative functional neuroimaging studies. *Human Brain Mapping*, *25*, 46–59.
Padmala, S., & Pessoa, L. (2011). Reward reduces conflict by enhancing attentional control and biasing visual cortical processing. *Journal of Cognitive Neuroscience*, *23*, 3419–3432.
Parvizi, J., Rangarajan, V., Shirer, W. R., Desai, N., & Greicius, M. D. (2013). The will to persevere induced by electrical stimulation of the human cingulate gyrus. *Neuron*, *80*, 1359–1367.
Paulus, F. M., Krach, S., Blanke, M., Roth, C., Belke, M., Sommer, J., et al. (2015). Fronto-insula network activity explains emotional dysfunctions in juvenile myoclonic epilepsy: Combined evidence from pupillometry and fMRI. *Cortex*, *65*, 219–231.
Peelle, J. E., McMillan, C., Moore, P., Grossman, M., & Wingfield, A. (2004). Dissociable patterns of brain activity during comprehension of rapid and syntactically complex speech: Evidence from fMRI. *Brain and Language*, *91*, 315–325.
Pierrot-Deseilligny, C., Rivaud, S., Gaymard, B., & Agid, Y. (1991). Cortical control of reflexive visually-guided saccades. *Brain*, *114*, 1473–1485.
Postle, B. R., Berger, J. S., & D'Esposito, M. (1999). Functional neuroanatomical double dissociation of mnemonic and executive control processes contributing to working memory performance. *Proceedings of the National Academy of Sciences, U.S.A.*, *96*, 12959–12964.
Procyk, E., Ford Dominey, P., Amiez, C., & Joseph, J. P. (2000). The effects of sequence structure and reward schedule on serial reaction time learning in the monkey. *Cognitive Brain Research*, *9*, 239–248.
Rottschy, C., Langner, R., Dogan, I., Reetz, K., Laird, A. R., Schulz, J. B., et al. (2012). Modelling neural correlates of working memory: A coordinate-based meta-analysis. *Neuroimage*, *60*, 830–846.
Rushworth, M. F., Walton, M. E., Kennerley, S. W., & Bannerman, D. M. (2004). Action sets and decisions in the medial frontal cortex. *Trends in Cognitive Sciences*, *8*, 410–417.
Schaefer, A., Kong, R., Gordon, E. M., Laumann, T. O., Zuo, X. N., Holmes, A. J., et al. (2018). Local-global parcellation of the human cerebral cortex from intrinsic functional connectivity MRI. *Cerebral Cortex*, *28*, 3095–3114.
Shenhav, A., Botvinick, M. M., & Cohen, J. D. (2013). The expected value of control: An integrative theory of anterior cingulate cortex function. *Neuron*, *79*, 217–240.
van der Kouwe, A. J. W., Benner, T., Salat, D. H., & Fischl, B. (2008). Brain morphometry with multiecho MPRAGE. *Neuroimage*, *40*, 559–569.
Wager, T. D., & Smith, E. E. (2003). Neuroimaging studies of working memory: A meta-analysis. *Cognitive, Affective & Behavioral Neuroscience*, *3*, 255–274.
Woolgar, A., Jackson, J., & Duncan, J. (2016). Coding of visual, auditory, rule, and response information in the brain: 10 Years of multivoxel pattern analysis. *Journal of Cognitive Neuroscience*, *28*, 1433–1454.
Yeo, B. T., Krienen, F. M., Eickhoff, S. B., Yaakub, S. N., Fox, P. T., Buckner, R. L., et al. (2015). Functional specialization and flexibility in human association cortex. *Cerebral Cortex*, *25*, 3654–3672.
Yeo, B. T., Krienen, F. M., Sepulcre, J., Sabuncu, M. R., Lashkari, D., Hollinshead, M., et al. (2011). The organization of the human cerebral cortex estimated by intrinsic functional connectivity. *Journal of Neurophysiology*, *106*, 1125–1165.
Zekveld, A. A., Rudner, M., Kramer, S. E., Lyzenga, J., & Rönnberg, J. (2014). Cognitive processing load during listening is reduced more by decreasing voice similarity than by increasing spatial separation between target and masker speech. *Frontiers in Neuroscience*, *8*, 88.